Supplementary Information

Monolithic Photonic Architecture for Volumetric Illumination in Plasmonic Photocatalysis

Abraham J. Offen, Wenhao Li, Dmitrii Tsvetkov, Jiawei Liang, Yogendra Kumar Mishra, Natalia M. Litchinitser, Jie Liu*

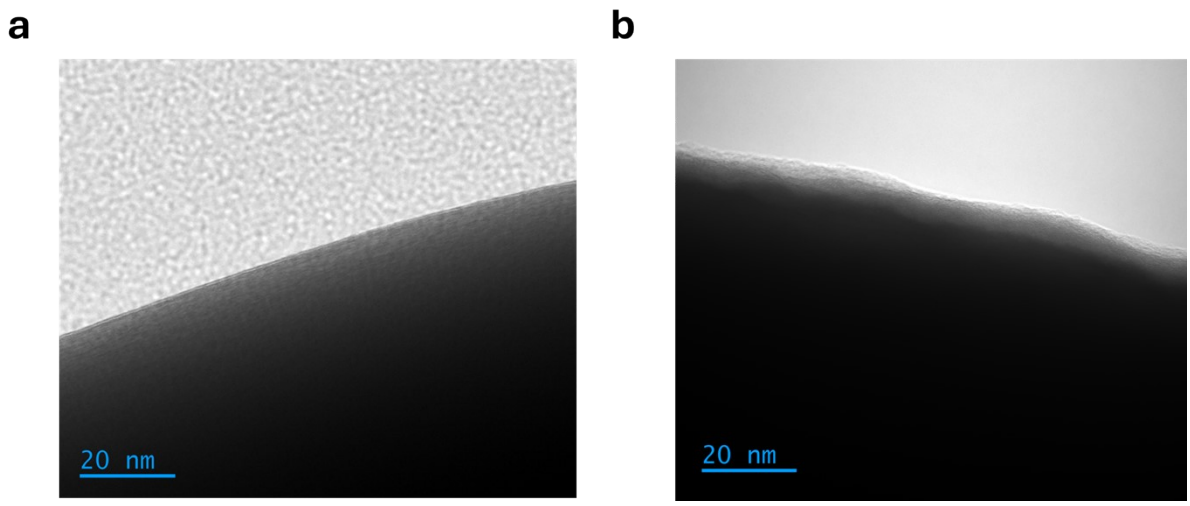

Figure S1. TEM images of **(a)** pristine ZnO surface and **(b)** TiO_2-coated ZnO surface. TiO_2 samples were not further pursued for catalytic and optical measurements but rather used as proof of concept illustrating the ease of surface modification.

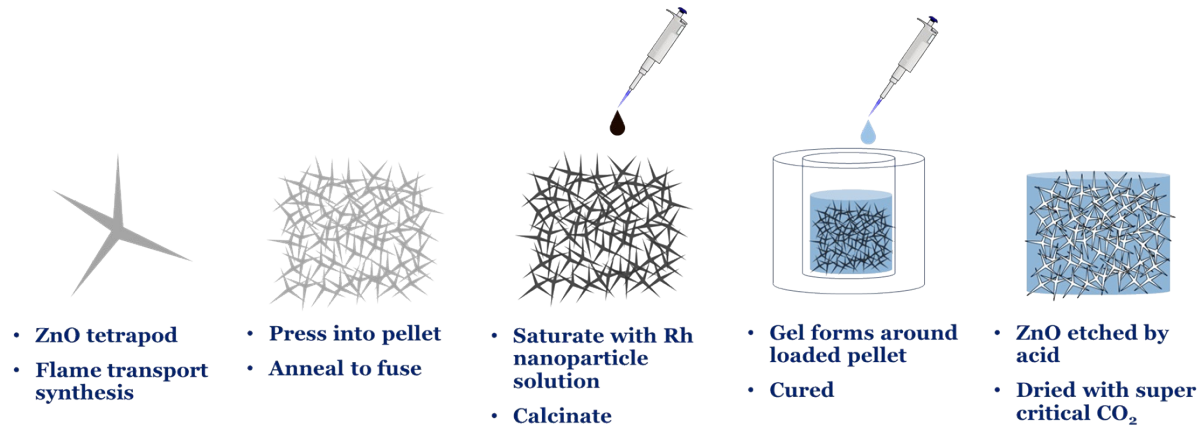

Figure S2. Synthetic diagram for monolithic catalysts.

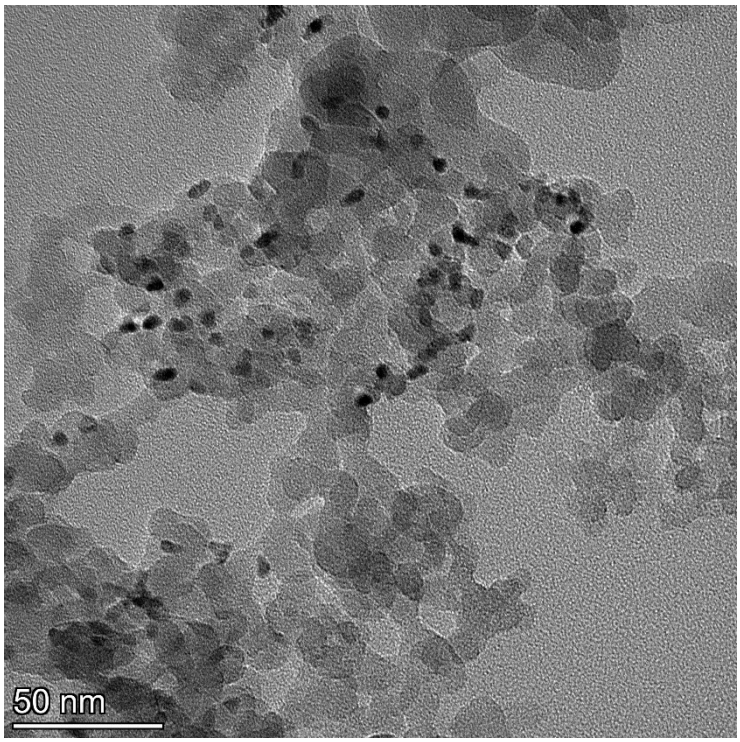

Figure S3. TEM image of Rh/SiO_2-PEA catalyst pellet. For loading onto the TEM grid, the monolith was necessarily ground, destroying the novel porous structure. The Rh nanoparticles are clearly visible amongst the aerogel fragments.

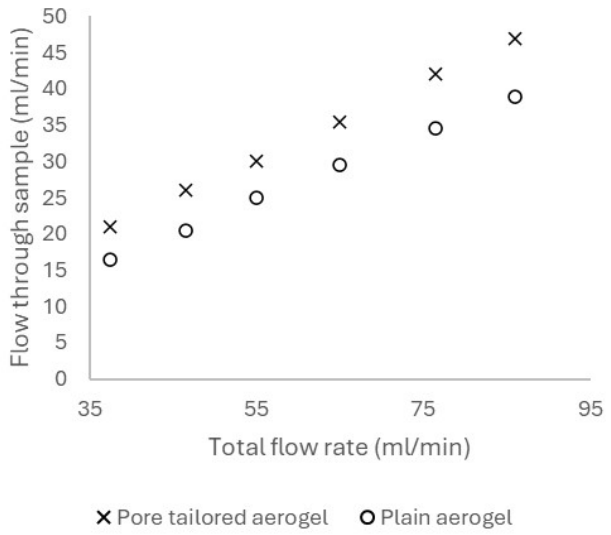

Figure S4. Comparison of mass flow between the modified aerogel made using a sacrificial ZnO template and a pristine aerogel. A stream of N_2 was split into two identical paths each containing a sample holder loaded with either the modified or pristine aerogel followed by a flow meter.

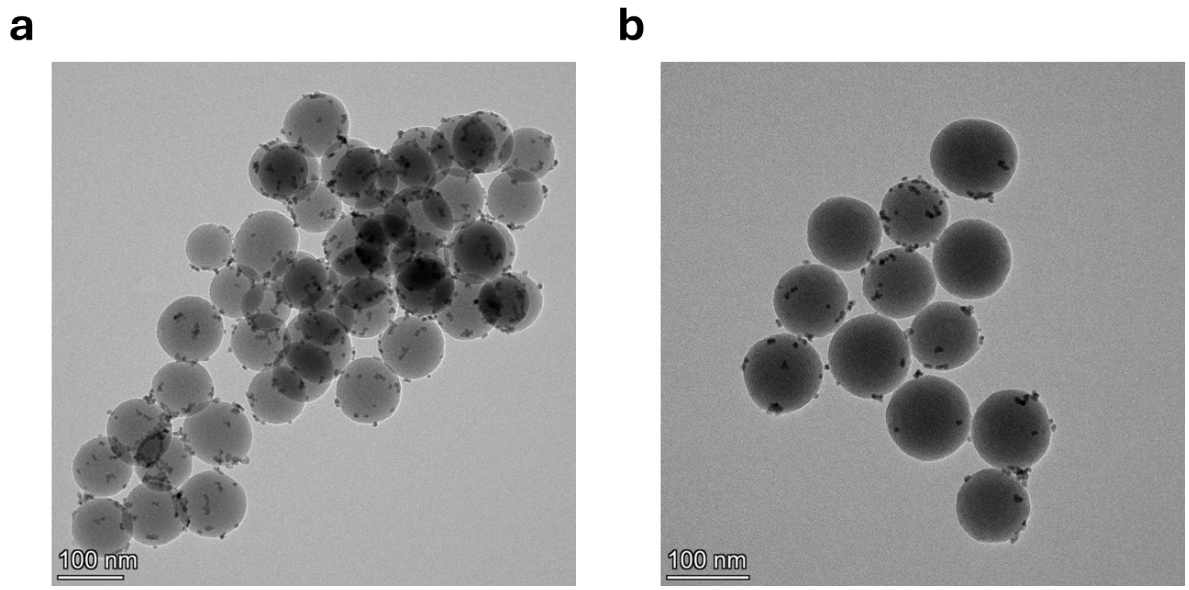

Figure S5. **(a)** TEM image of Rh/SiO_2-S, powder with Rh concentrated to 6.5 mg SiO_2 placed on the surface, **(b)** TEM image of Rh/SiO_2-H, powder with equivalent volumetric loading across 20 mg SiO_2.

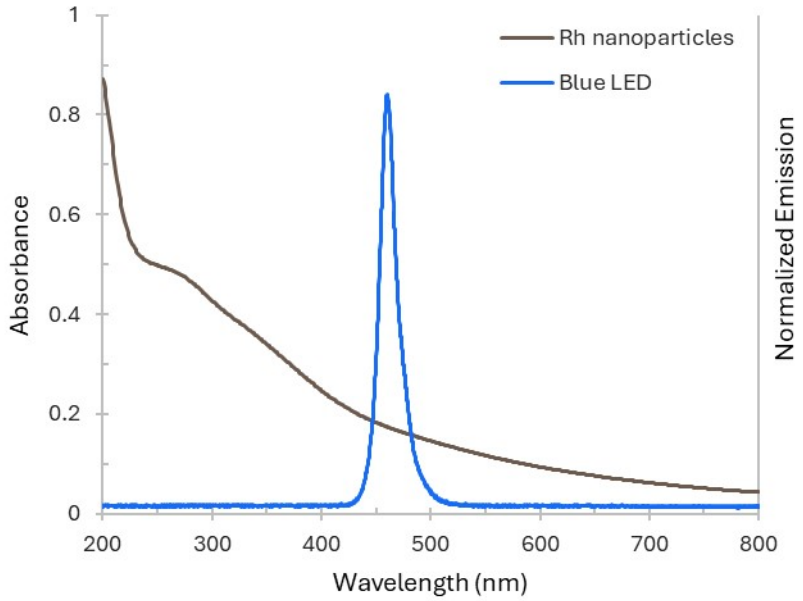

Figure S6. Absorption spectrum of Rh nanoparticles in ethanol overlayed with the emission spectrum of the fiber coupled blue LED.

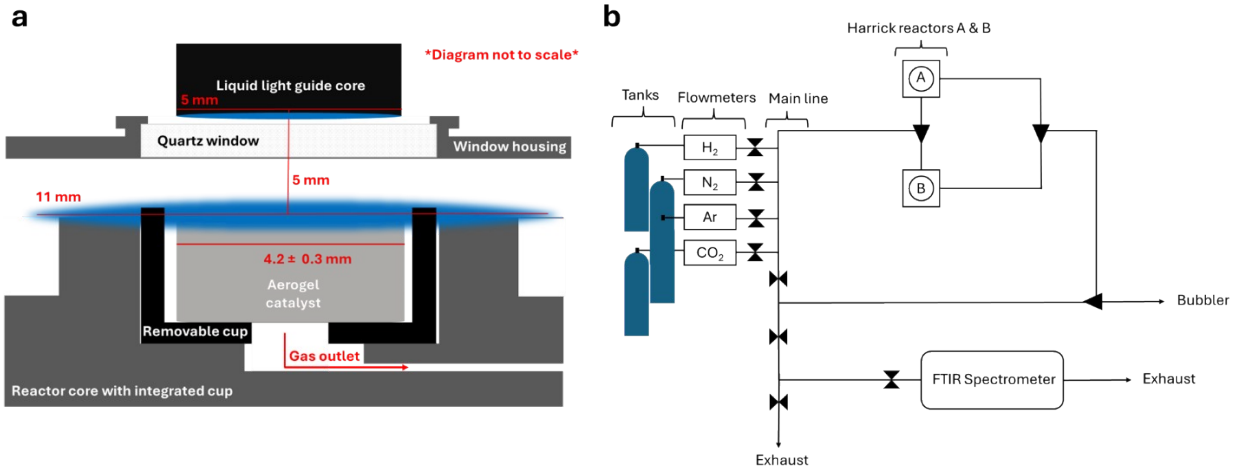

Figure S7. **(a)** Diagram of the illuminated Harrick Raman high pressure reactor loaded with an aerogel sample. **(b)** Diagram of the catalytic reactor gas and measurement system; reactor B was used for all experiments.

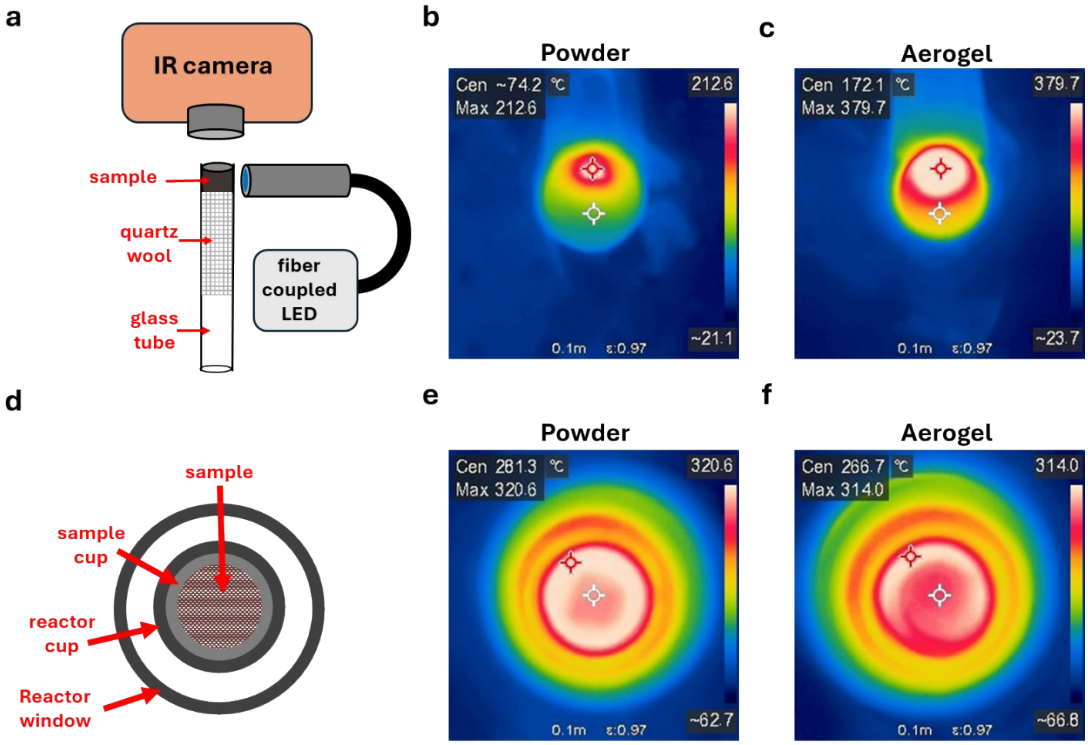

Figure S8. **(a)** Measurement diagram of photothermal energy produced by illumination of the Blue LED **(b)** uniformly loaded powdered Rh/SiO_2 catalyst **(c)** porous aerogel catalyst loaded with 0.7% Rh **(d)** Measurement diagram of thermal energy from the reactor heater. **(e)** Uniformly loaded powdered Rh/SiO_2 catalyst **(f)** porous aerogel catalyst loaded with 0.7% Rh. Measurements are considered qualitative due to the limited resolution of the HSF Tools HF96 thermal camera used.

1. $CO_{2(g)} + 2\ * \rightleftharpoons CO* + O*$ Dissociative adsorption
2. $H_{2(g)} + 2\ * \rightleftharpoons 2H*$
3. $CO* \longrightarrow CO_{(g)} + *$ RDS for CO
4. $CO* + H* \rightleftharpoons CHO* + *$
5. $CHO* + * \longrightarrow CH* + O*$ RDS for CH_4
6. $O* + H* \rightleftharpoons OH* + *$
7. $OH* + H* \rightleftharpoons H_2O_{(g)} + 2*$
8. $CH* + H* \rightleftharpoons CH_2* + *$
9. $CH_2* + H* \rightleftharpoons CH_3* + *$
10. $CH_3* + H* \rightleftharpoons CH_{4(g)} + 2*$

Figure S9. Competing mechanisms of CO_2 evolution on plasmonic Rh catalyst as proposed in ref. 12. * denotes a surface binding site.

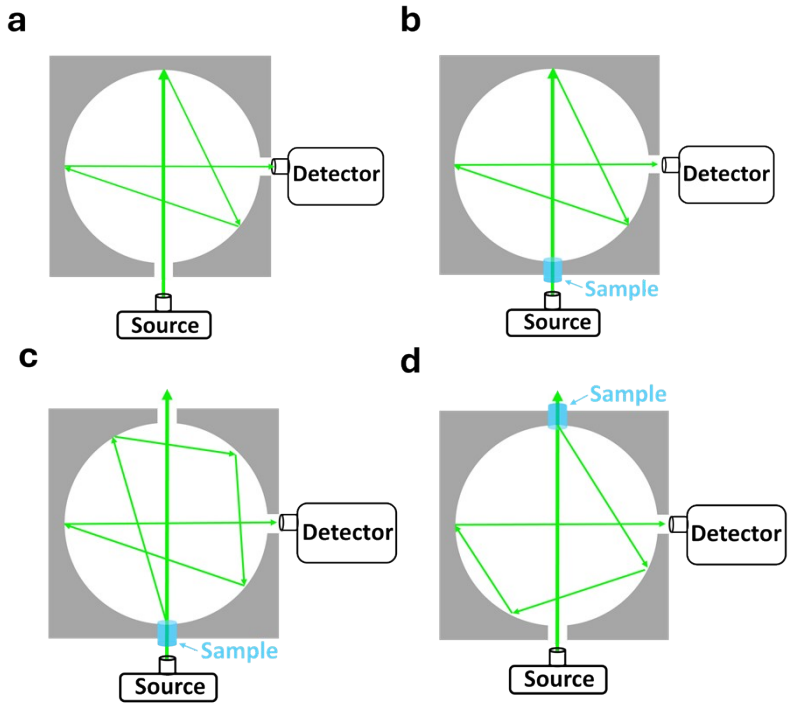

Figure S10. Measurement diagram of **(a)** total power, allows for normalization of transmission, diffusion and reflection data **(b)** sample transmittance, the sum of direct and scattered transmission, **(c)** sample diffusion measures light scattered by the samples internal structure **(d)** sample reflection measures reflected light, enables calculation of absorption coefficient.

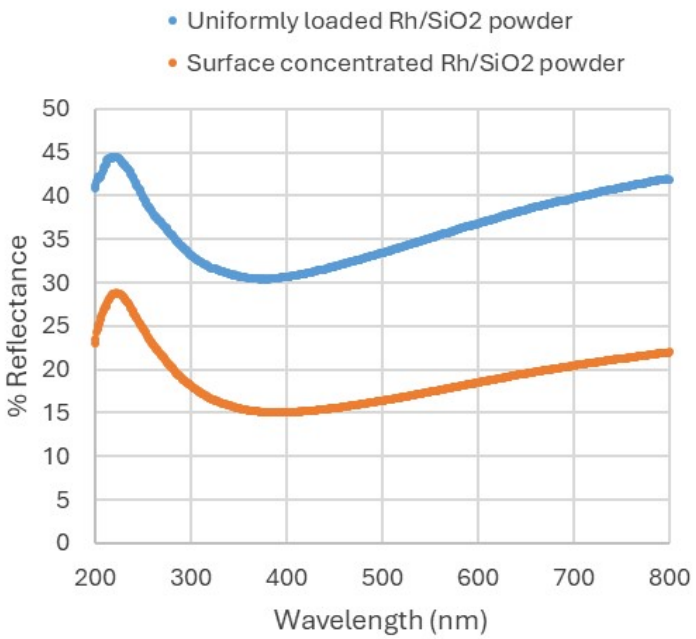

Figure S11. Reflectance measurements of the powdered Rh/SiO_2 catalysts.

Table S1. Cumulative distribution fit

Sample	λ (95% confidence interval)	R^2
0.4 wt. %	1.067 (1.051 1.082)	0.9886
1.7 wt. %	1.932 (1.925 1.939)	0.9995

Monolithic architecture	Synthetic conditions	Source of porosity	Porosity	Loaded absorber	Relative visible reflectance	Relative density	Performance analysis	Ref.
Ni foam – dip coated	Purchased	Purchased foam	mm scale	$In_2O_{3-x}(OH)_y$	High - reflective reactor	Moderate	CO_2 reduction	39
Reticulated α-Al2O3 foam	Purchased	Purchased foam	mm scale	none	High – reflective reactor	Moderate	Bulk optical simulation	40
Zirconia foam – dip coated	Purchased	Purchased foam	mm scale	Cu-doped TiO_2	High – reflective reactor	Moderate	CO_2 reduction	48
Bundled quartz tubes – dip coated	Purchased tubes	Gaps between tubes	mm scale	Cu-doped TiO_2	Low – reflective reactor	High	CO_2 reduction & bulk optical simulation	48
"Waveguide photoreactor" quartz rods – roll coated	Purchased rod	Gaps between nanorods	nm-μm scale	$In_2O_{3-x}(OH)_y$	Low-reflective reactor	High	CO_2 reduction	41
Inverse opal	Mild – sol gel	Sacrificial PS nanospheres	nm scale	Au nanoparticles	Size dependent – slow photons improve abs.		2,4-dichlorophenol degradation	49
SiO_2 opal	Mild – sol gel	Gaps between nanospheres	nm scale	Ag nanoparticles	Size dependent – slow photons improve abs.	Moderate	H_2 production (sacrificial MeOH)	50
SiO_2 opal – This work	Mild – sol gel	Gaps between nanospheres	nm scale	Rh nanoparticles	High	Moderate	CO_2 reduction	N/A
Boron nitride "artificial solid fog"	Highly sensitive	Sacrificial ZnO tetrapods	μm scale – very high	none	Low	Ultra-low	Optical analysis	54
SiO_2 "aeroglass"	Mild	Sacrificial ZnO tetrapods	μm scale – very high	rGO flakes	Low	Ultra-low	Optical & photothermal analysis	55
$Ce_{1-x}Zn_xO_{2-\delta}$ "aeroglass"	Mild	Sacrificial ZnO tetrapods	μm scale – very high	Rh nanoparticles	Low	Ultra-low	Gas flow analysis	56
TiO_2 aerogel –surface functinalized	Harsh & sensitive –sol gel	Native pores	nm scale	Pd, PdAu, nanoparticles	Low	Low	H_2 production	43
SiO_2 aerogel	Mild – sol gel	Native pores	nm scale	TiO_2 nanoparticles	Low	Low	Phenol degradation	47
TiO_2 aerogel on 3D printed template	Harsh & sensitive –sol gel	3D printed template	mm and nm scale	Pd nanoparticles	Low	Low	H_2 production	44
This work (pore enhanced aerogel) – drop cast	Mild – sol gel	Sacrificial ZnO tetrapods	μm and nm scale - high	Rh nanoparticles	Low	Low	CO_2 reduction & bulk optical	N/A

simulation

Table S2 Comparative overview of selected monolithic optically designed photocatalysts. This non-exhaustive table is color coded by architecture type. Key trends including pore nature, use of reflective reactors, and bulk optical simulations are noted where applicable. Density can be a proxy for ease of handling since denser optical monoliths are generally sturdier.